

Experimental and computational analysis of initiation and propagation of shear bands in bulk metallic glasses

ABEYGUNAWARDANA-ARACHCHIGE, G <<http://orcid.org/0000-0001-8989-4132>>, NEKOUIE, Vahid and BELL, Andy

Available from Sheffield Hallam University Research Archive (SHURA) at:

<https://shura.shu.ac.uk/30432/>

This document is the Published Version [VoR]

Citation:

ABEYGUNAWARDANA-ARACHCHIGE, G, NEKOUIE, Vahid and BELL, Andy (2019). Experimental and computational analysis of initiation and propagation of shear bands in bulk metallic glasses. *Materials Research Express*, 6 (7): 075207. [Article]

Copyright and re-use policy

See <http://shura.shu.ac.uk/information.html>

PAPER

Experimental and computational analysis of initiation and propagation of shear bands in bulk metallic glasses

To cite this article: G Abeygunawardana-Arachchige *et al* 2019 *Mater. Res. Express* **6** 075207

View the [article online](#) for updates and enhancements.

You may also like

- [Amorphous phase formation rules in high-entropy alloys](#)
Qiu-Wei Xing, , Yong Zhang et al.
- [Recent development of chemically complex metallic glasses: from accelerated compositional design, additive manufacturing to novel applications](#)
J Y Zhang, Z Q Zhou, Z B Zhang et al.
- [Mechanisms of compressive deformation and failure of porous bulk metallic glasses](#)
S Gouripriya and Parag Tandaiya



ECS Membership = Connection

ECS membership connects you to the electrochemical community:

- Facilitate your research and discovery through ECS meetings which convene scientists from around the world;
- Access professional support through your lifetime career;
- Open up mentorship opportunities across the stages of your career;
- Build relationships that nurture partnership, teamwork—and success!

Join ECS!

Visit electrochem.org/join





PAPER

Experimental and computational analysis of initiation and propagation of shear bands in bulk metallic glasses

RECEIVED
18 October 2018REVISED
15 March 2019ACCEPTED FOR PUBLICATION
27 March 2019PUBLISHED
10 April 2019G Abeygunawardana-Arachchige¹ , Vahid Nekouie¹ and Andy Bell²¹ Wolfson School of Mechanical, Electrical and Manufacturing Engineering, Loughborough University, Leicestershire, United Kingdom² MSC Software, Frimley, Surrey, United KingdomE-mail: aravindaousl@gmail.com**Keywords:** shear bands, free volume, strain gradient theory, nonlocal plasticity, wedge indentation, finite element analysis, bulk metallic glass**Abstract**

Shear bands (SBs) play a key role in the mechanical deformation of Bulk Metallic Glasses (BMGs). The key to obtaining an insight into the shear band mechanism is to understand the root cause of shear band initiation and propagation. SB initiation is a difficult event to capture, considering the negligible macroscopic ductility of BMGs. It is the premature shear localisation in the nano scale which is responsible for the noticeable brittle nature in the macro-scale. Plastic deformation of BMGs occurs due to the formation of highly localised SBs of approximately 10–20 nm in thickness. These then propagate at a velocity of around 100 ms^{-1} and results in catastrophic failure in both tension and compression due to the micro-cracks formed through the coalescence of the nano voids. This study develops a technique to capture the early initiation of SBs through a wedge indentation test. The work found that incremental loading (a definite load applying incrementally by 1 kN in stages) did not affect the overall mechanical response of the BMG material, indicating that SB evolution can be examined with an incremental indentation test. A predictive numerical model for SB initiation and propagation in BMGs is presented using two approaches: a strain gradient model and an integral-type non-local approach employing the Vermeer–Brinkgreve modelling strategy (Strömberg, Ristinmaa 1996). Comparisons are made between the outcomes of physical tests and numerical modelling to obtain an insight into the relative merits.

1. Introduction

Bulk metallic glasses (BMGs) are amorphous metals which are relatively new class of engineering materials possessing unique set of chemical, physical and mechanical properties. They are manufactured through a quenching process that prevents forming long range atomic order which characterise metals. BMGs consists of elements interact with primary metallic bonds (Greer *et al* 2013).

It is well established today that BMGs deformation dominate with Shear Bands (SBs) mediated plasticity, and recently it was well established a connection between number density of SBs at a notch tip and K_{IC} (Narayan *et al* 2018). One of the main obstacles to their widespread use is the absence of a fundamental structural theory to describe their deformation behaviour. The concept of a shear transformation zone (STZ) by Argon (Argon 1979) and the work of Spaepen (Spaepen 1977) advanced the understanding somewhat. However, STZ could not be identified as a structural state associated with the atomic configuration of BMGs. The notion of free volume emerged from the work of Spaepen was subsequently developed to a level that it could be considered a structural state variable. Several authors (Dai 2012, Greer *et al* 2013) have proposed that strain localisation occurs easily by free-volume disordering; increase of free volume due to deformation. In a recent advancement, the idea of ‘glass dislocations’ (Nelson 1983) has been applied (Acharya and Widom 2017) to understand the micro-scale structural deformation of BMGs.

Experimental investigation of SBs initiation requires careful procedures due to advanced sample preparation/fabrication requirements. The main difficulty with experimental observation stems from the

extremely small thickness of SBs (around 20 nm) and also their transient nature (nanosecond time scale) (Greer *et al* 2013). Currently due to the technological limitation, SB initiation and propagation can only be analysed 'ex situ' and cannot be analysed 'in situ'. This is mainly due to the above mentioned transient nature of SB initiation. Some *in situ* methods available are acoustic emission and high speed camera. However have several disadvantages; high sensitivity for temporal resolution and inability to obtain SB development without shear offset respectively (Xie *et al* 2018). Therefore, numerical simulation has turned out to be not only an attractive, but also probably the only way to understand SBs. In fact, our main objective in this presented work is to predict the initiation and propagation of shear bands with numerical simulation. In addition, it is still not known yet (in indentation of BMGs) if SBs initiate from surface of the sample/within a location of the sample volume or, from both locations simultaneously. Hence our secondary objective is to study the propagation directions of SBs in localised deformation such as indentation.

Representation of initial free volume content is important in a model as it governs micro scale as well as macro scale softening. Free volume of BMG specimen is generated by the quench process during manufacturing of BMGs and grows when the specimen is subjected to mechanical deformation (Li and Li 2007). Amount of free volume retained in liquid phase of BMG is much higher than the solid phase. It has been found that concentration of free volume rely upon the quenching process such that decrease of free volume, for decrease in cooling rate and vice versa (Lu *et al* 2018). Though their concepts of a shear transformation zone and free volume remain relevant, the models presented by Spaepen and Argon were one-dimensional and hence could not capture the 3D stress-strain states (Cheng and Ghosh 2013). Among the 3D finite deformation models available in the literature, only the work by Yang (Yang *et al* 2006) and Vaidyanathan (Vaidyanathan *et al* 2001) provides hints toward recent developments in this area. The former work is based on the von Mises failure criterion with free-volume dependent viscoplasticity taken into account. The approach has the advantage of capturing features over a wide range of temperatures and hence is able to reproduce experimentally observed stress-strain curves. Furthermore, recent experimental indentation results indicate that the von Mises criteria are inadequate to describe the deformation of BMG (Cheng and Ghosh 2013). Vaidyanathan compared the experimental nano-indentation behaviour of Vitreloy-I with those predicted by simulations and found a good correlation using the Mohr-Coulomb criterion. Work of Vaidyanathan (Vaidyanathan *et al* 2001) and Zhang (Zhang *et al* 2003) also confirms the influence of hydrostatic pressure on fracture surface orientation and yielding. Recently Cheng (Cheng and Ghosh 2013) proposed a constitutive framework incorporating finite deformation kinematics, the Mohr-Coulomb criterion and a kinetic law that governs evolution of the density of free volume. Their work can explain the transition between inhomogeneous and homogeneous deformation.

Initiation of a SB is an important event when modelling deformation of BMGs as it can give rise to a sequence of phenomena such as flow localisation, SB propagation, nano-void formation, and coalescence, leading to a macro scale fracture. In the macro scale, negligible plasticity of BMGs compared to a crystalline material, is caused by early initiation of flow localisation. There is still a lack of understanding of mechanisms responsible for the initiation and propagation of SBs at the micro scale. Defining micro-plasticity for Metallic Glass is not sincere as crystals; since there are atomically disordered structures of a glass for local plastic transition at any stress. For instance, there is evidence of irreversible atomic rearrangement even well below the macroscopic yield stress (Maa β and Derlet 2018). These are most likely to be SB formation as a result of complex loading geometries.

In present work an alternative technique based on a phenomenological constitutive model to predict the initiation and propagation of SBs originating beneath the indenter is presented. The approach is able to capture the initiation and propagation of the SBs in BMGs adequately (detailed experimental work is available in (Nekouie *et al* 2018)). The model based on the experimental observation of Nekouie *et al* has provided new insights into SB initiation and propagation in Zr-Cu based BMGs under inhomogeneous loading conditions. To validate the numerical model, a wedge indentation experiment was carried out.

2. Materials and experimental procedure

A Zr-Cu based BMG with a nominal composition Zr₄₈Cu₃₆Al₈Ag₈ (at%) was selected for this study which was produced at IFW Dresden of Institute for Complex Materials, Germany. The supplied samples were sectioned using wire electric discharge machining (EDM) into rectangular specimens of approximately 40 mm × 5 mm × 2 mm. All samples were polished to a mirror finish before experimentation and their structure was inspected using x-ray diffraction (XRD) (Rigaku Ultima-III diffractometer) with a Cu-K α radiation target. To study SB evolution, an interrupted wedge indentation procedure was performed on a BMG specimen. The high-speed steel (HS 6-5-4) wedge indenter was designed and manufactured in-house (see figure 1) to have a 60° wedge angle and a 19.5 μ m edge radius. The tests were conducted with an Instron 3345

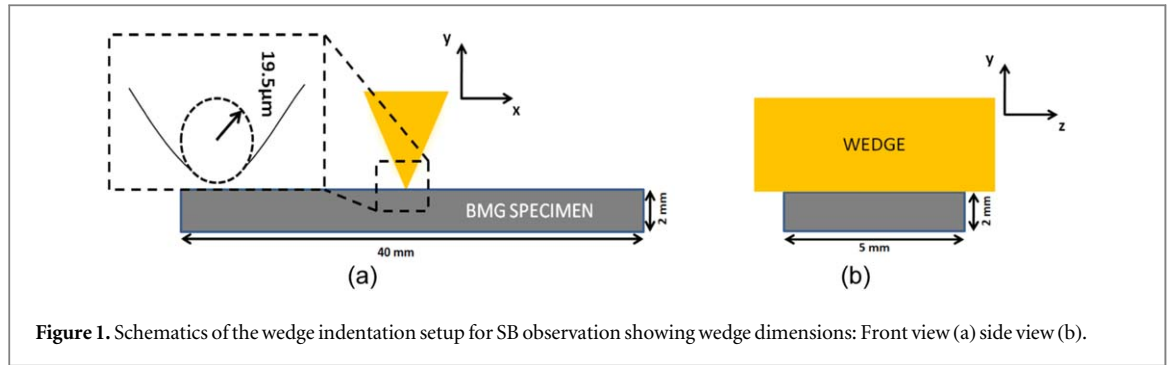


Figure 1. Schematics of the wedge indentation setup for SB observation showing wedge dimensions: Front view (a) side view (b).

testing machine using a displacement rate of 0.5 mm min^{-1} and an applied load range of 1 kN–3 kN with 1 kN increments (Nekouie *et al* 2018).

3. Theoretical background

Continuum models developed to describe material deformation behaviour can be divided into three main categories as strictly local, weakly non-local and strongly non-local theories (Bazant and Jirásek 2002). Strictly local (also referred to as classical plasticity) models, consider stress at a point which uniquely depends on the current deformation or its history at that point only, and hence the effect of length scale, which represent the size of localisation zone, is not included. When the tangent stiffness modulus are non-positive definite, the damage zone volume reduces to zero. Hence the structure fails at zero energy dissipation even though the energy per unit volume is finite. As a remedy, a constraint on the Finite Element (FE) solution is essential to account for the diminishing element size. This inherent FE mesh dependent deformation localization can be removed by considering a length scale (l). A constitutive model that incorporates l is commonly referred as a non-local model. In these, l reflects the transmission of micro structural information to the neighbouring points within a certain distance. A variety of models developed to describe metal plasticity already incorporates l (Aifantis 1984, Fleck and Hutchinson 1993, Fleck *et al* 1994, Tveergard and Needleman 1995)). We have exploited l in the current model to implement aspects of strain gradient theory and Integral type non-local theory to capture the early localisation event.

3.1. Local/classical models for plasticity

Classical constitutive plasticity models in differential forms are always treated as strictly local. Several experimental studies on the tensile (θ_T) and compressive (θ_c) fracture angles of BMGs by Donovan (Donovan 1988) and Zhang (Zhang *et al* 2003) indicate that deformation and fracture of BMGs do not obey the von Mises criterion. The observed fracture angles in the range of $0^\circ < \theta_T < 45^\circ$ and $45^\circ < \theta_c \leq 50^\circ$, indicate that normal stress plays an important role in addition to the shear stress. In this study, the Drucker-Prager (DP) yield criterion is used which is a pressure dependent model incorporating both von Mises and hydrostatic stresses. The DP failure criterion is implemented through user subroutines of the MSC Marc software and can be defined as follows (Toi *et al* 2004):

$$\sigma_{eq} = \sqrt{\frac{3}{2} \sigma'_{ij} \sigma'_{ij}} - 3\phi p \quad (1)$$

Where, σ_{eq} is the equivalent stress, σ'_{ij} the deviatoric stress components, ϕ the material property and p the hydrostatic pressure. The first term after the equality symbol represents the von Mises stress. An associated flow rule is used to define the plastic strain increment of the material. One drawback in classical plasticity in studying micro/nano-scale phenomenon is, it lack length scale in it description to reflect the transmission of micro structural information to the neighbouring points. The expression (1) represents strictly local behaviour and several additional terms are required to account for the non-local behaviour.

3.2. Strain-gradient theory

Strain-gradient theory help refine the kinematic description of the model by capturing the spatial resolution of the material not solely by conventional strain, but also by strain gradients (second derivatives of displacement). This way the stress evaluation is guided by both material properties and the local neighbourhood points. Since the neighbourhood is arbitrarily small, these models are termed weakly non local.

The strain-gradient concept is widely used in crystal plasticity theory to include the length scale which captures material size effects (Fleck and Hutchinson 1993). Here, the strain-gradient approach is used in

particular to localise deformation softening at points which represent the free volume of the BMG specimen. Calculation procedure of the strain gradient at each gauss point ($\nabla\gamma^{(i)}_G$) is illustrated using the following pair of equations:

$$\nabla\gamma^{(i)}_G = \frac{\partial\gamma^{(i)}_G}{\partial x} = \frac{\partial\gamma^{(i)}_G}{\partial(\psi)} \frac{\partial(\psi)}{\partial x} = \sum_{i=1}^n (\nabla_\psi N^i(\psi) \gamma^{(i)}_N) J^{-1}. \quad (2)$$

$$J = \frac{\partial x}{\partial(\psi)} = \sum_{i=1}^n (Y^i N^i(\psi) \nabla_\psi) \quad (3)$$

Where ∇_ψ is the Nabla operator, J^{-1} the inverse of the Jacobian, $\gamma^{(i)}$ the equivalent plastic strain components at each i^{th} gauss points, $N^i(\psi)$ the shape functions ∇_ψ the natural co-ordinate system and Y^i the location of integration points with respect to the natural co-ordinate system. The resultant strain gradient $\nabla\gamma^i_R$ can be computed using

$$\nabla\gamma^i_R = \sqrt{\left(\frac{\partial\gamma^i}{\partial x}\right)^2 + \left(\frac{\partial\gamma^i}{\partial y}\right)^2 + \left(\frac{\partial\gamma^i}{\partial z}\right)^2} \quad (4)$$

The gradient dependent yield criterion (F) can be expressed as

$$F = \sigma_{eq} - \sigma_y(1 + (\nabla\gamma^i_R \times l)) \quad (5)$$

Where σ_y is the yield stress, σ_{eq} the equivalent stress and l the length parameter necessary to adapt the yield criterion in order to be dimensionally consistent.

3.3. Integral type non-local plasticity theory

The numerical material model was implemented using the integral-type non-local plasticity theory in which the constitutive law at a given point of a continuum was applied using the weighted averages of a state variable over a certain neighbourhood of that point. A linear formulation that combines a local softening variable with a non-local softening variable (Vermeer-Brinkgreve model) (Strömberg and Ristinmaa 1996, Rolshoven 2003) was used in the following way

$$\hat{\kappa} = m\bar{\kappa} + (1 - m)\kappa \quad (6)$$

Where $\bar{\kappa}$ is the non-local parameter, κ the local parameter and m a parameter that governs the degree of local or non-local nature of parameters used in the formulation. In this study, the local parameter is considered to be the strain gradient at each integration point. The yield criterion incorporates integral type non local theory where parameter m binds the portions of weak ($m = 0$) and strong ($m = 1$) non-local effects (term *weak* implies that strain gradients at several integration locations around the material point are incorporated in the calculation whereas *strong* non-local behaviour means that the effect of strain gradients of all integration points within a volume of a sphere at a material point is considered). The numerical range of m is restricted to 0 and 1. Several test simulations were performed with m values other than the above values but the yielded results did not provide any physical meaning considering that m in the ranges; $m < 0$, $0 < m < 1$, $1 < m$ represent a mix of both weak and strong non-local behaviour. To include the decay of interaction effects with distance between two points, a non-local average function $\alpha_\infty(x_0, x)$ is used. The non-local average, $\bar{\kappa}$ of a local field $\kappa(x)$ is defined as (Strömberg and Ristinmaa 1996)

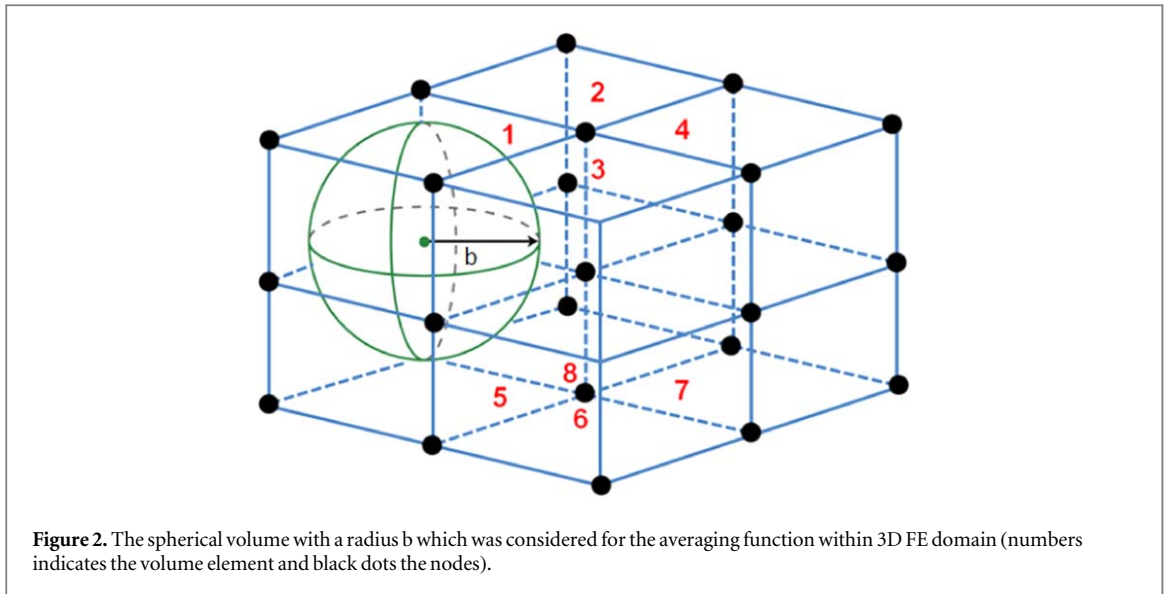
$$\bar{\kappa}(x) = \frac{\int_V \alpha_\infty(x_0, x) \kappa(x) dx}{\int_V \alpha_\infty(x_0, x) dx}. \quad (7)$$

The function $\alpha_\infty(x_0, x)$ was selected such that the impact of the local variable κ is inversely proportional to the distance between x and x_0 .

The averaging function therefore is expressed as

$$\alpha_\infty(x_0, x) = \begin{cases} \exp\left(-\frac{\|x_0 - x\|}{b}\right) & \text{if } \|x_0 - x\| \leq b \\ 0 & \text{if } \|x_0 - x\| \geq b \end{cases} \quad (8)$$

which is valid within a chosen sphere of influence of radius b (figure 2). Equation (7) can be written as follows in terms of the finite-element mesh discretization (Qu *et al* 2015):



$$\bar{\kappa}(x) = \frac{\int_V \alpha_\infty(x_i, x_j) \kappa(x_j) dx}{\int_V \alpha_\infty(x_i, x_j) dx} = \frac{\sum_{j=1}^N w_j \alpha_\infty(x_i, x_j) \kappa(x_j) V_j}{\sum_{j=1}^N w_j \alpha_\infty(x_i, x_j) V_j} = W_{ij} \kappa_j, \quad (9)$$

Where the weighting function W_{ij} is defined as

$$W_{ij} = \frac{w_j \alpha_\infty(x_i, x_j) V_j}{\sum_{j=1}^N w_j \alpha_\infty(x_i, x_j) V_j}. \quad (10)$$

Here, N is the number of integration points within the domain and $\alpha_\infty(x_i, x_j)$ can be used to calculate the averaging function between i th and j th integration points. The variable w_j represents the weighting coefficient at the j th integration point. The yield criterion can then be derived as

$$F = \sigma_{eq} - (1 - m)H\kappa_i - mHW_{ij}\kappa_j - \sigma_y, \quad (11)$$

where H is the hardening modulus.

4. 3D Finite-element model

The constitutive models were implemented on the MSC Marc 2014.1 non linear Finite Element (FE) software platform through a set of user-defined subroutines. The deformation regime was studied using 3D continuum elements with adaptive re-meshing. The extent of free volume or weak-site was determined as a percentage of the total sample volume. They were in-cooperated in the FE model by random generation; hence discrete deformation can be obtained. Similar approach was considered by (Yu *et al* 2017) to simulate rolling on BMGs, though the plasticity model was not analogous to us. These weak-sites defined the fluctuation of free volume or chemical heterogeneity of the BMG specimen and controlled the energy barrier of SBs (Nekouie *et al* 2018). As reported by Nekouie (Nekouie *et al* 2018), SBs are mostly initiated from these weak sites. The implemented constitutive framework used the Drucker-Prager yield criterion to represent hydrostatic effects and an exponential softening law to model the disordering process of the free volume. The framework involves strain gradient theory and integral type non-local approach to improve the resolution of non-homogeneous deformation fields. The numerical model was validated against the experimental results obtained from wedge indentation tests.

4.1. Wedge indentation

Wedge indentation is a novel technique used to overcome some well-known limitations of nano and micro-indentations. In a traditional indentation experiment, SBs are not easily visible since they occur within the material volume below the indenter. Therefore, wedge indentation was employed here to observe the evolution of SBs in the BMG specimen volume by carefully studying the orthogonal plane of the indentation. The wedge is made of high speed steel with a 60° wedge angle and $19.5 \mu\text{m}$ tip radius. The dimension of the BMG specimen tested was approximately $40 \text{ mm} \times 2 \text{ mm} \times 5 \text{ mm}$.

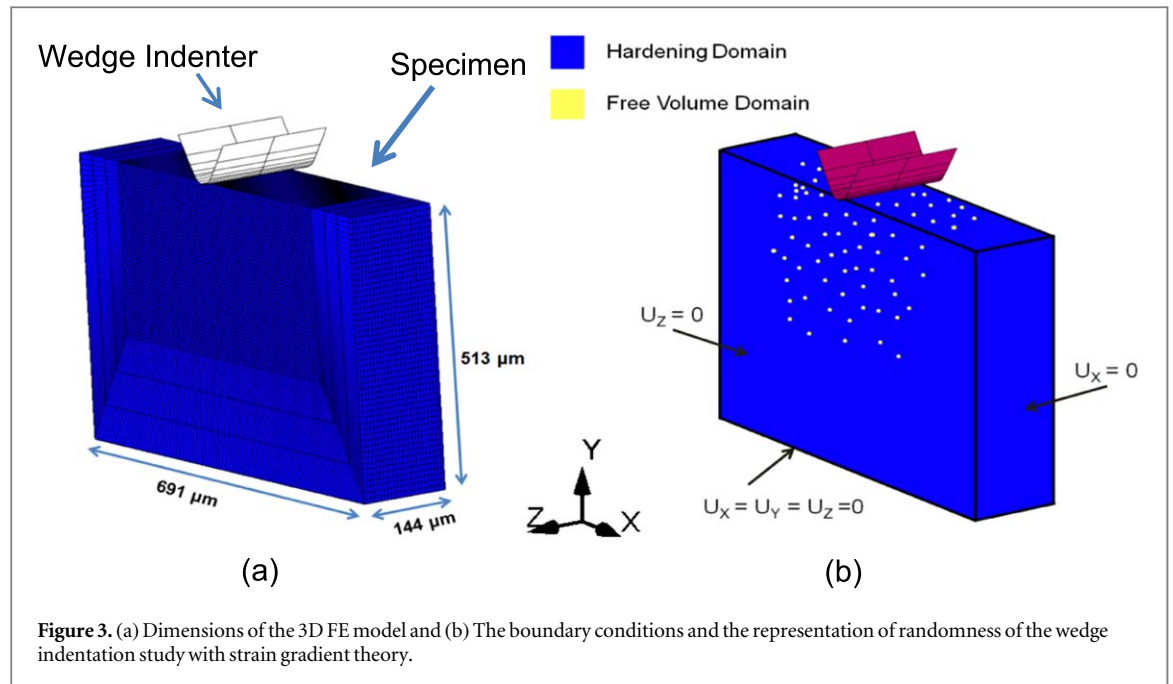


Figure 3. (a) Dimensions of the 3D FE model and (b) The boundary conditions and the representation of randomness of the wedge indentation study with strain gradient theory.

4.1.1. FE Model development

The 3D FE model of the wedge experiment was developed as shown in figure 3(a). The BMG specimen size was limited to a volume of $144 \mu\text{m} \times 513 \mu\text{m} \times 691 \mu\text{m}$ for computational efficiency. The 3D FE model consists of approximately 10^5 hexahedral elements with a finer mesh (element size of $6.25 \mu\text{m}$) at the region of contact with the indenter. The mesh size of $6.25 \mu\text{m}$ was decided after mesh sensitivity analysis. Our studies show that the chosen mesh is sufficient to capture SB propagation in the material. To depict free volume sites, spatially random locations in the model were assigned with exponentially softening post yield properties while the surrounding regions are represented by a linear hardening bulk domain as shown in figure 3(b). It was shown by our experimental studies (Nekouie *et al* 2018) on nano-indentation of individual SBs that higher displacement was recorded up to peak load than those made in the bulk materials, which indicate SBs were softer and should be a softening domain under deformation. Automatic mesh refinement was not considered on the elements representing free volume, with it being activated only on the surrounding bulk matrix when the material point reached to plastic state. It is because a local inelastic constitutive law at that region with strain softening damage will lead to spurious localization of damage into zero volume with zero strain energy with small mesh size. Upon mesh refinement of the softening elements, it will converge to a solution with vanishing energy dissipation in structural failure (Bazant 1976). In free volume regions, upon softening, the lowest stress level was prevented from becoming negative. We assumed that free volume content may not migrate within the material volume under inelastic state. Even if this is the case, we would not expect our observations/conclusions to be noticeably different. Furthermore Liu (Liu *et al* 2010) claims based on their study that overall plastic deformation and the ultimate strength are determined by SB propagation rather than the nucleation of embryonic bands and limited influence of sample surface concern that the initiation of SB is mainly governed by the intrinsic structures and properties of BMGs. The thickness of the SB in the FE model is governed by the mesh refinement level. Local adaptive remesh technique available in MSC Marc was used to refine when equivalent plastic strain of a certain integration point reach to 0.01. The value was used to settle both computational power and SB thickness after careful observation of the equivalent plastic strain contours. The indenter was considered as a rigid contact body with the geometry identical to the indenter used in experiments.

Dai and co-workers (Dai *et al* 2005, Dai and Bai 2008, Jiang and Dai 2009) presented a coupled thermo-mechanical deformation of BMG undergoing 1D shear deformation. Their analysis revealed that production of free volume aided the abrupt increase in the temperature before the instability. Their work led to an expression for the onset condition for—SB instability and the internal scales involved in the coupling softening instability; were converted into internal free—volume and thermal scales. Dai (Dai 2012) measured the internal length scale and represent whether the instability would occur easily or not; it was shown that the internal time scale and measured how fast the instability initiates with free volume/thermal softening or softening based on both. It was also shown that the internal scales will decrease as the strain rate increases and the internal free-volume length and time scales are well below those for the thermal softening case, indicating that shear instabilities caused by free-volume creation occurred much easier and faster than in the thermal softening case. At low strain rates the thermal internal scale and time scale is very large and, hence thermal strain softening occurs with great difficulty.

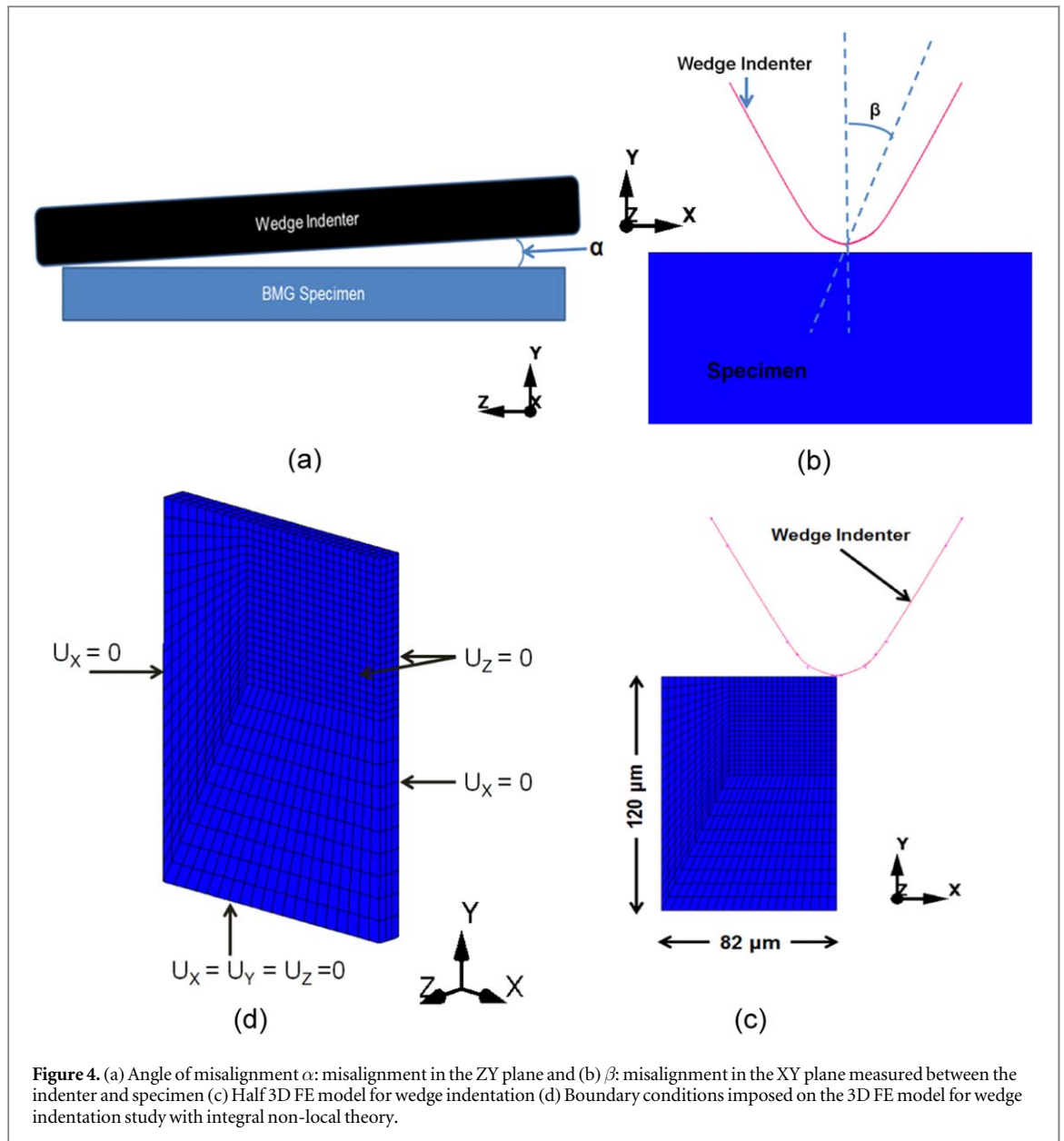


Figure 4. (a) Angle of misalignment α : misalignment in the ZY plane and (b) β : misalignment in the XY plane measured between the indenter and specimen (c) Half 3D FE model for wedge indentation (d) Boundary conditions imposed on the 3D FE model for wedge indentation study with integral non-local theory.

Since—SB instability occurs even at quasi static loading, it is probable that the strain localisation initiates from free-volume softening. Based on the above analysis it was decided that thermal softening could be disregarded.

Appropriate boundary conditions are imposed to represent the physical experiment. Both Z faces (front and back face) were constrained in displacement in the Z direction ($U_z = 0$) and X faces (right and left faces) were constrained in displacement in the X direction ($U_x = 0$). Bottom of the specimen was constrained in all three displacement directions ($U_x = U_y = U_z = 0$) (figure 3(b)).

Misalignment of the indenter with work piece plays an important role in micro indentation. The effect of misalignment of the indenter on the force-deflection response is studied by varying the angle α and β , as shown in figures 4(a) and (b).

The algorithm for non-local plasticity is computationally expensive. Hence, effort was concentrated more in the vicinity of the indentation (figure 4(c)) half of the domain was modelled (figures 4(d) and (c)) with an element length of $2.5 \mu\text{m}$. To surpass this, other efficient computational procedure is warranted in future studies, thus non-local plasticity can be used for much larger size FE model.

For numerical analyses, a series of studies were conducted on several model parameters and the misalignment angles α and β to determine the material properties that would be in best agreement with the experimental results (table 1).

Angle β did not effect to the simulation results significantly, hence β was considered to be $\sim 0^\circ$. The initial free volume content was considered to be at a low percentage (2% of the material volume) which remained at that level during the deformation regime. The parametric studies revealed that the overall result would not be

Table 1. Materials and Simulation Parameters used in the Analysis.

E (GPa)	ν	σ_y (MPa)	μ	H (MPa)	α (°)	β (°)	Φ
70	0.35	1.85	0.1	200	0.2	0	0.16

affected even though the volume was significantly increased. The flow stress of the free volume sites was set to decrease exponentially to 80 MPa from the initial yield stress of 1850 MPa, and remain at that value. This reduction of flow stress would occur within an equivalent plastic strain range of 0.0–0.5.

5. Results and discussion

TEM studies showed that only broad amorphous peaks were present and no indication of crystallinity was found through the presence of Bragg's peaks (see Nekouie *et al* 2018). As reported by Nekouie *et al* dark field TEM images also confirmed the absence of crystalline phases in the sample and Selected Area Diffraction (SAED) pattern showed only a set of diffused rings typical for an amorphous structure of glassy nature. Characterisation of SBs with TEM also confirmed an amorphous structure with no evidence of nano-sized crystallites.

5.1. Experimentation with micro wedge indentation.

As stipulated by Liu, (Liu *et al* 2010) mechanical response of a BMG specimen which is subjected to an external stress can be classified into three different stages: an elastic region, an intermediate region with rapid strain hardening, and a steady state plastic deformation region (perfect plastic). Following the elastic region, there is a clear evidence that the specimen analysed in this work is in the rapid strain hardening condition of the final deformation stage.

In the single loading mode, the desired load level is reached by a single indenter displacement whereas in incremental loading, the same load level as the single mode is applied but by increments of 1 kN. The measured indentation imprints for single (2 kN) and incremental loading (1, 2 kN) showed that the difference in the indentation widths for the two modes was less than 5%. A similar result was obtained with 3 kN and 1, 2, 3 kN loading in the single and incremental modes, respectively. In contrast to micro- and nano-indentation, the results demonstrated that wedge indentation was capable of providing an incremental study of SB propagation. Figure 5(b) presents the incremental indentation test using loads from 1 kN to 3 kN with a 1 kN increment of 1 kN performed at the same location as the single mode. As can be seen in figure 6(b), the incremental loading has not affected the overall mechanical response of BMG, indicating that the evolution of deformation can be examined with an incremental indentation test. As shown in the inset figure 5(b), the residual imprints of the indenter for the first (1 kN) and second (1–2 kN) incremental loading were approximately 22 μm and 50 μm , respectively. As shown on the force-displacement curve (figure 5(b)), the initial displacements of the indenter in order to be reengaged with the specimen in the second (1–2 kN) and third (1–2–3 kN) incremental loading were also equal to 22 μm and 50 μm , respectively. Hence, it can be concluded that the incremental load-displacement curve is reasonable and repeatable, and the area underneath the load-displacement curve can be used to calculate the work done for the total deformation including elastic, plastic and damage deformations.

5.2. Influence of strain-gradients on shear band initiation and propagation under non-homogeneous deformation: Analysis with strain gradient plasticity.

The primary motivation for performing wedge indentation was to characterise the initiation of SB within the material volume. Figure 6(a) compares the force-displacement (F-D) curves of the wedge indentation by experiments and simulation. The results are in good agreement with the experiment. The initial discrepancy up to a displacement of $\sim 16 \mu\text{m}$ is due to misalignment α (figure 5(a)) of the wedge indenter. Simulations with zero misalignment show that the expected maximum force would be higher by $\sim 54\%$ than the current maximum force. The effect of μ is not clearly visible due to the misalignment. This demonstrates the significance of the misalignment of the indentation setup on the results. Figure 7(a) illustrates the SB patterns propagated inside the specimen volume as well as on the surface of the specimen. It is clear that SBs on different cutting planes have distinct patterns. This is due to the random distribution of the free volume sites in the material volume. Randomness of the free volume sites governs the density of SBs as well as the propagated patterns. Figure 7(c) shows that SBs are not initiated on a plane that lies along the length of the wedge indenter. This was observed in our experiments as on (Nekouie *et al* 2018). The effect of strain gradients on the initiation and propagation of SBs were studied and the load-displacement curves for different length parameters (l) were compared with the experiment. (Figure 6(b)).

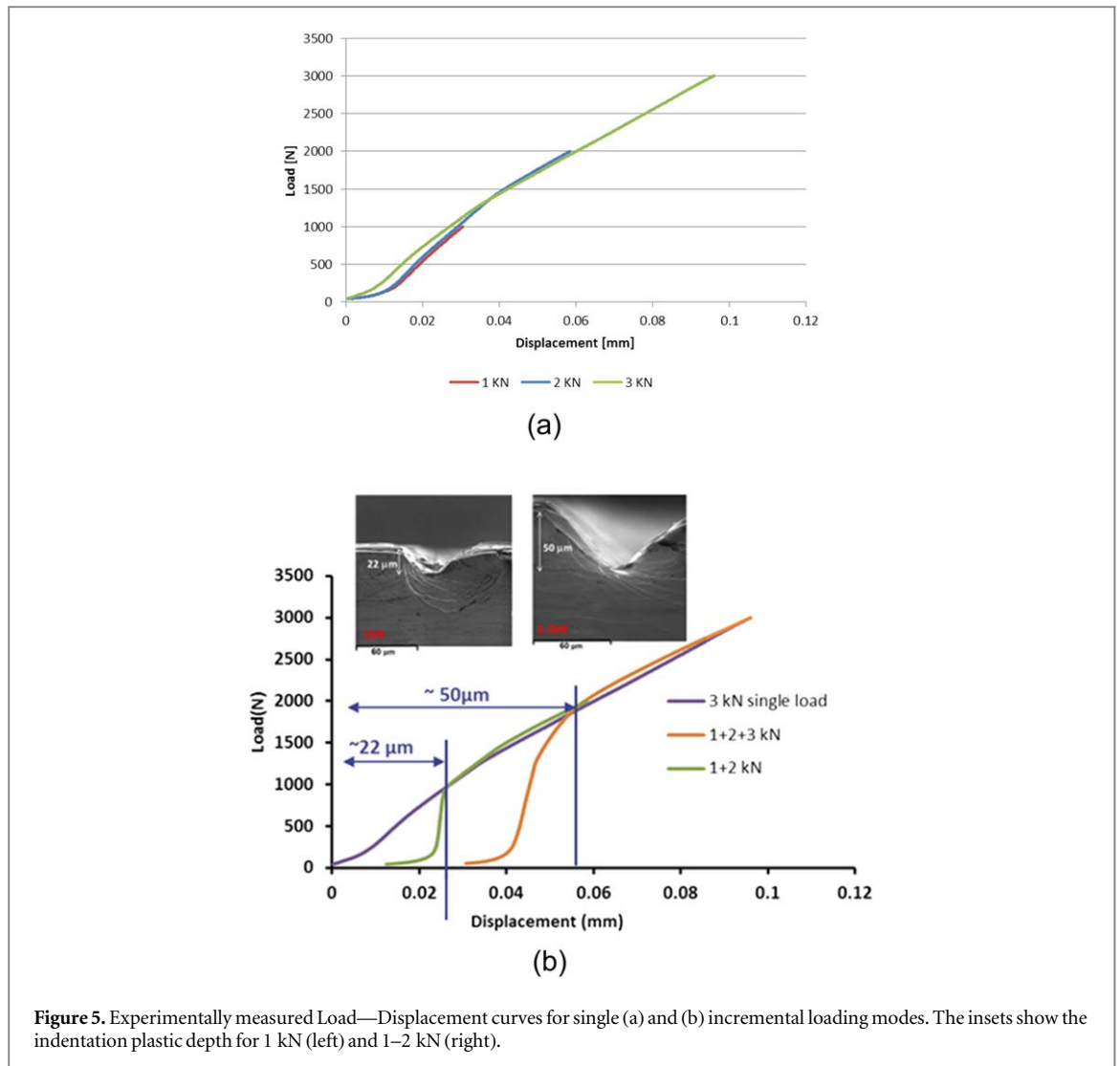


Figure 5. Experimentally measured Load—Displacement curves for single (a) and (b) incremental loading modes. The insets show the indentation plastic depth for 1 kN (left) and 1–2 kN (right).

Though free volume softening is exponential, experimental observation reveals (figure 6(b)) that force increases with displacement. This is due to the fact that the flow stress of the material domain surrounds free volume sites that rise linearly with no constraint; hence the hardening response dominates the softening response from the F-D curve. Similar observation was noted experimentally by Liu and Co-workers (Liu *et al* 2010) that this strain hardening occurs due to the energy barrier of Shear Transition Zones (STZ). At micro level, energy barrier level varies within the material volume due to amorphous nature. At ‘weak sites’ due to lower energy barrier, activates initially and gets exhausted with the deformation. These ‘weak sites’ controls the energy barrier for operation of SBs. Once these ‘weak sites’ with low energy barrier get exhausted; much higher loads are required to overcome ‘weak sites’ with large energy barrier.

Figure 7(b) clearly distinguishes some slight differences in the equivalent plastic strain results. Nevertheless, comparing figures 7(a) and (b), it is obvious that the plastic strain distribution is not significantly affected by the strain gradients. The evidence originating from figures 6(b) and 7(b) could lead to the fact that the strain gradient effect arising from internal material behaviour is not observed as a dominant factor in SB initiation and propagation for indentation processes. This may be due to the indentation, by nature, being leading to a non-homogeneous deformation that induces a strain gradient because of the tip geometry. We believe it is this effect that causes the strain gradients to arise and to a lesser extent due to differences in the material constitutive description between the bulk and the free volume.

Figure 8 elaborate the series of SB initiation and propagation events with the displacement during the wedge indentation. Equivalent plastic strain of value greater than 0.05 was initially observed when the indenter was displaced 6 μm from the FE model. The effect of the misalignment of the wedge indenter would be clear from figure 8(a) that portion of the volume marked in red colour has yielded initially. This confirms wedge initially contact this surface and later the other surfaces as the indenter displaced. Major SBs was observed from the surface when the indenter was displaced by 14.3 μm and later number of SBs were initiated and propagated on

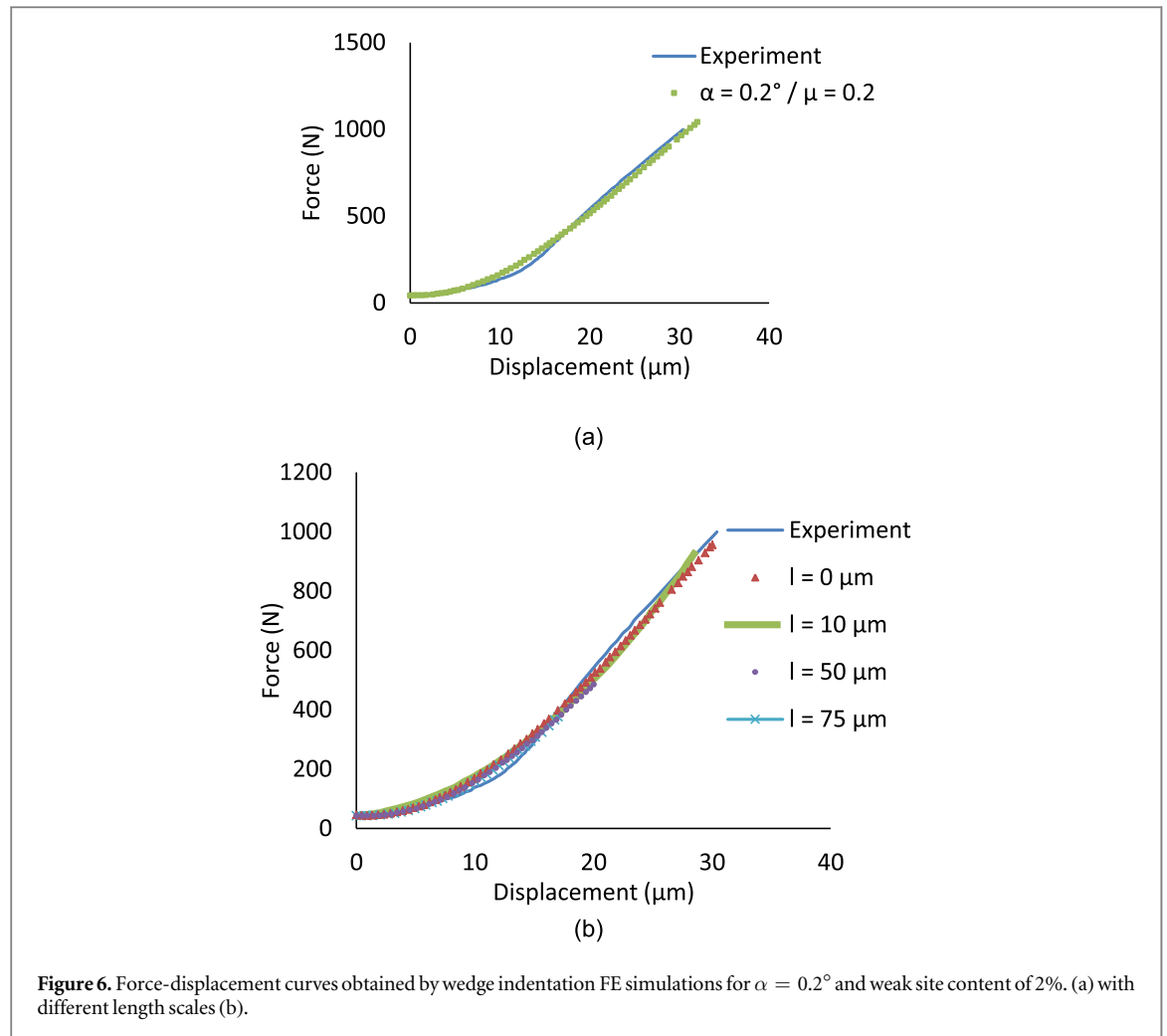


Figure 6. Force-displacement curves obtained by wedge indentation FE simulations for $\alpha = 0.2^\circ$ and weak site content of 2%. (a) with different length scales (b).

various directions. It is learned from the FE model that propagation directions cannot be quantitatively predicted as it depends on the distribution of free volume (density of free volume) of the indenting material volume. It is also observed that considering the area underneath the indenter surfaces (wedge surfaces), the sample surface will yield to much higher level for higher friction coefficient values. This occurs due to large friction forces in addition to the normal forces due to indentation. Under these circumstances, it is clear that plastic strain initiating from these regions would continue to propagate into the specimen volume and combine with the other softening volumes (free volume) beneath the surface. It is equally important to note that surface roughness of the sample will play a major role in experiment setup as SB may originate from locations with greater surface roughness and propagate to inner domain to combine with SBs originated from free volume (in the material domain). These locations on the specimen surface are stress raisers (stress concentration) and impact adversely on the post indentation analysis of SBs. Hence surface preparation (polishing) is highly warranted prior to experiment studies of BMGs. From figures 8(c) and (d) it is further shown of localised yielded locations. These locations are free volumes regions (represented as strain softening elements) and it is clear on our second objective of the study that SBs are initiated due to strain localization originating from both free volume locations within the general material volume (under the indenter tip) and plastic strain originated from the surface of the specimen simultaneously. Apparently, if there are surface discontinuities (stress raisers) or free volume zones adjacent to the indenter/specimen interface, we believe SBs would have already initiated and propagated and would not be visible even in the SEM images due to crushing downward movement of the material volume close to the indenter tip. This is also clear from the insets from figure 5(b). From our FE models, free volume zones were included close to the specimen surface (figure 3(b)). Notwithstanding for the shown equivalent plastic strain region (shown in legend) SBs are not shown for low displacement of the indenter but is significant when the indenter is reached 25 μm and 30 μm . (figures 8(e), (f)). In aid of this, we believe that SBs can still be formed underneath the indenter in simulations but need more resolution in the mesh to visual representation. More resolution accompanies more computational cost.

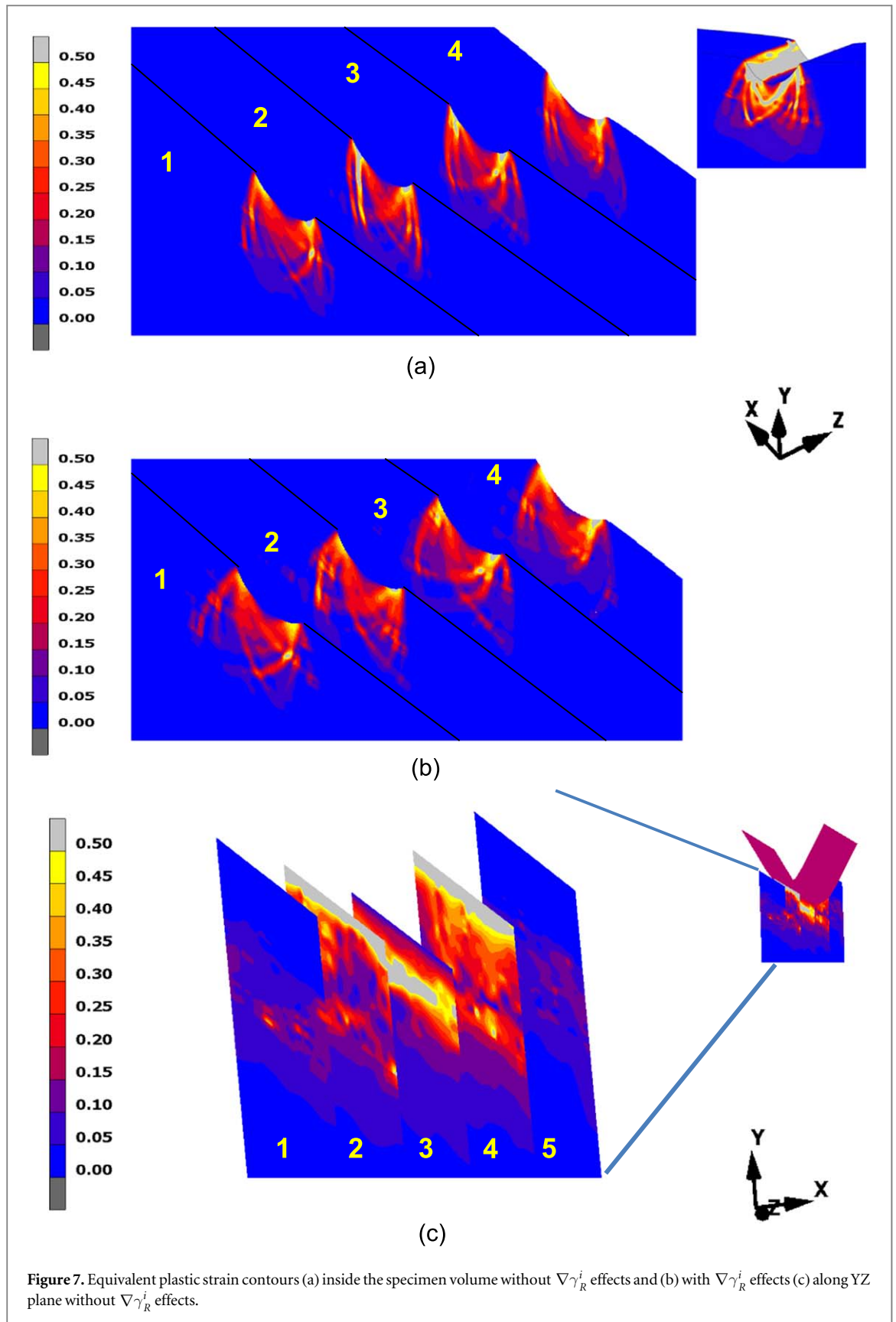


Figure 7. Equivalent plastic strain contours (a) inside the specimen volume without $\nabla\gamma_R^i$ effects and (b) with $\nabla\gamma_R^i$ effects (c) along YZ plane without $\nabla\gamma_R^i$ effects.

5.3. Influence of strain-gradients on shear band initiation and propagation under non-homogeneous deformation: Analysis with integral non-local plasticity.

As mentioned, an important part of our study in integral non-local plasticity is the Vermeer-Brinkgrave model. According to equation (10), for strong integral non-local plasticity, radius 'b' of the sphere (figure 2) was chosen

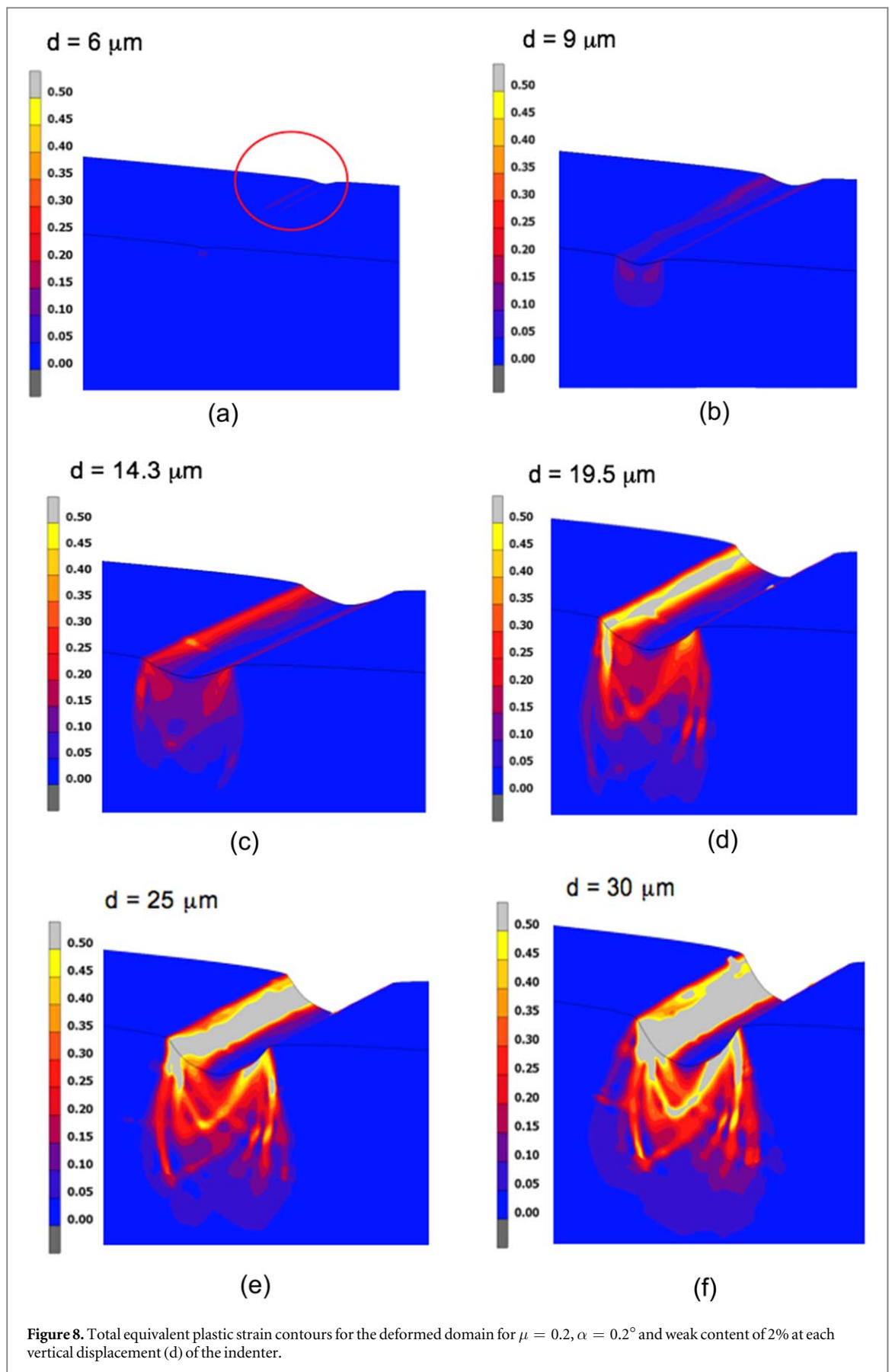


Figure 8. Total equivalent plastic strain contours for the deformed domain for $\mu = 0.2$, $\alpha = 0.2^\circ$ and weak content of 2% at each vertical displacement (d) of the indenter.

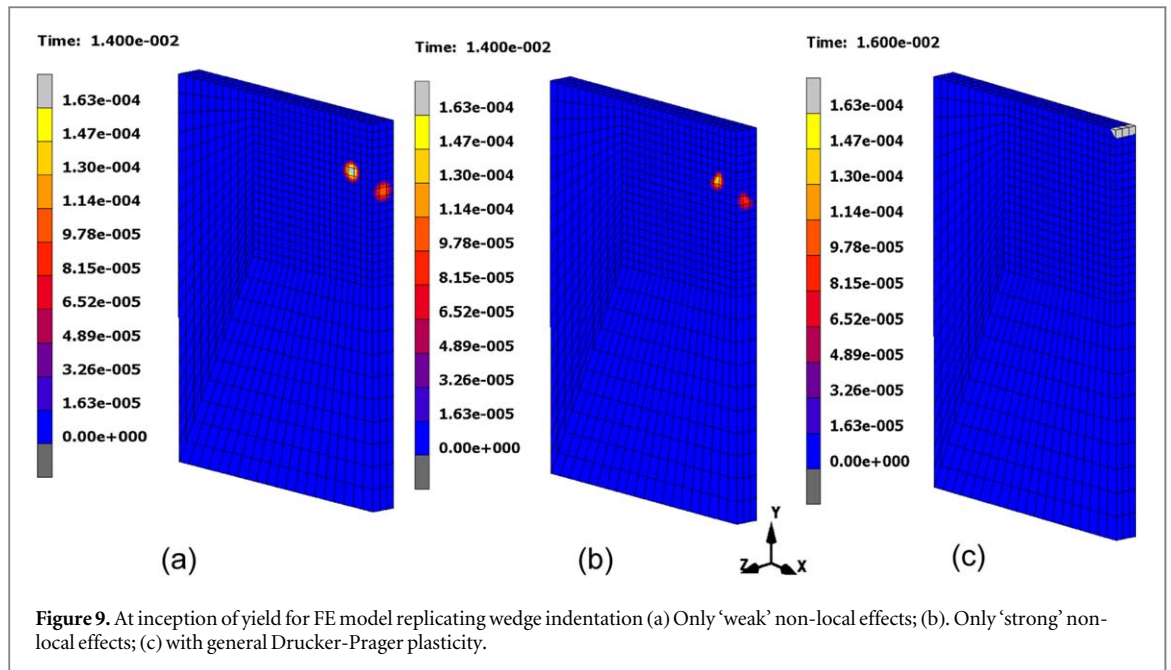


Figure 9. At inception of yield for FE model replicating wedge indentation (a) Only ‘weak’ non-local effects; (b). Only ‘strong’ non-local effects; (c) with general Drucker-Prager plasticity.

such, the whole FE model was enveloped by the sphere (figure 4(d)). The local variable κ is chosen to be the strain gradient at each integration point within the envelope.

It is not possible to compare the experimental work directly with the non-local plasticity procedure, mainly due to the restriction of FE model size by virtue of expensive nature of the computational procedure. It was observed that the model (figure 9(c)) with conventional plasticity yielded plastically at a higher load and occurred directly underneath the indenter. For studies on ‘weak’ non-local and ‘strong’ non-local plasticity analyses (figure 9(a),(b)), the initial yielding localised at the same loading level for both models, but at lower levels than the conventional plasticity (strictly local) model; occurring within the specimen volume (not particularly underneath the indenter). Nevertheless, correlating with the conventional plasticity, it is clear that onset of yield occurs earlier. It is apparent from this observation that ‘weak’/‘strong’ non-local integral plasticity models forecast early onset of plasticity for the BMG specimen at the micro scale compared to conventional plasticity. BMGs behaviour, at the micro scale, demonstrate significant plasticity and a narrow elastic region. This is mainly due to the abrupt initiation of SBs and their propagation. It is, therefore, reasonable to conclude that the significantly brittle nature (low elastic range) in the macro scale deformation of BMGs, is a direct result of the SBs originating at the micro scale. These SBs lead to distinct cracks and ultimately form a fracture surface. Since ‘strong’/‘weak’ non-local integral plasticity demonstrates early onset of plasticity we believe the procedure is suited for predicting micro scale plasticity and also explains the macro scale brittleness in BMGs. The computational procedure can be further developed to use in much larger FE models. This will aid us to predict SB initiation accurately like the current study but for much larger model and will be used to study in simulation of continuum scale engineering devices and MEMS devices made of BMGs. The observed behaviour through FE model using ‘weak’ and ‘strong’ non-local procedures are independent from the chemical composition of the BMGs; so as the mechanism of SB initiation and propagation at physical setup. The common deformation mechanism of BMGs as it would be is, it increases their internal free volume as they plastically deform, these dilatation causes nano-voids that ultimately leads to plastic deformation.

6. Conclusion

In this paper, we introduce an experimental technique and a numerical modelling scheme which model the initiation and propagation of SBs in BMG material, undergoing inhomogeneous deformations in micro scale. A relatively new technique, wedge indentation was employed for an incremental study of SB propagation. SB initiation and its propagation cannot be studied experimentally from ‘*in situ*’ techniques. Nearly all studies have the common trend; the patterns are observed and investigate in subsequent to SB propagation. This fact has led us to maneuver into simulation and numerical models; and is a convenient as well as necessary tool to perceive about inception and propagation of SBs. Numerical models accounting for the softening showed distinct SBs in wedge indentation studies on the surface as well as in the material volume. These SBs are restricted to a plane perpendicular to the wedge z axis (figure 1(b)) and not in parallel direction. The later observation can only be

noticed with simulations of numerical models; since SB observation within the material volume is still not yet possible with current instruments.

It was also observed from our numerical simulations that, under localised deformation, SB initiate from free volume zones beneath the indenter and plastic strain contours from the surface simultaneously and propagates along counter directions to form SBs. The study also indicated that misalignment of the indenter was the primary source of error which manifested in the recorded F-D curves, especially during the initial part of the indentation process. Complete elimination of misalignment of an indenter is a tedious process in experimental conditions. Numerical simulations play a major role to determine these issues.

Initiation and propagation of SBs for BMGs have a regular pattern and mechanism. Shear banding of BMGs are well known to be caused by free volume exist in the sample. Free volumes exist in BMG sample from its synthesis stage due to amorphous atomic arrangement and induce chemical heterogeneity. Resistance to deformation is reduced in these localised regions (softening) under loading. This resistance is considered to control the energy barrier for the operation of SBs (Nekouie *et al* 2018). In continuum scale, local yield stress of these 'weak sites' was used as the control parameter ('energy barrier') in the FE model. Since 'weak sites' represent within the bulk volume in continuum scale, our study considered similar yield stress in local as well as the bulk volume. However, the 'energy barrier' can be differed for each 'weak site' due to distinct free volume arrangements. The hardening response of overall F-D curve is due to the exhaustion of the lower-energy sites, and higher loads are required to activate other SBs with higher 'energy barrier'. It was clearly observed that SBs are onset from the 'weak sites' represented by the FE model, Plastic strain incurs by these 'weak site' are united with the plastic strain emanating from the surrounding 'weak sites', hence the inception of SB and propagation of these SBs linking each 'weak sites' depicts coalescence of free volume.

Three theoretical approaches (conventional plasticity, weak non-local plasticity and integral plasticity) were adopted in the study and all were computationally implemented using commercial FE code MSC Marc using user subroutines. One notable limitation of integral non-local model is the expensive nature of the computational procedure. More computational algorithms are warranted to improve computational cost.

It was shown, with the help of the integral non-local models, that for localised non-homogeneous deformation modes (indentation), yield initiation predicted earlier than the conventional and weak non-local plasticity approaches. As described in section 5.3, this observation endorses significant plasticity in micro scale and brittle behaviour in macro scale. The procedure specified in this work can be applied to study SB initiation and propagation in any type of BMGs under quasi-static loading conditions with different indenter geometries.

It can be concluded that integral non-local models are more efficient for predicting early onset of SBs in non-homogeneous deformation (such as indentation) than the conventional plasticity (strictly local) model and strain gradient plasticity models. The only limitation in the implementation of the integral non-local model currently is the high computational memory requirements.

For non-homogeneous deformation from the indentation, the strain gradient effects introduced by the 'weak' non-local material model were not significant compared to that of the gradient effects observed by virtue of the indenter tip's geometry. This was observed clearly by F-D curves and equivalent plastic strain contours. As a result, the length scale l was used more as a parameter to be dimensionally consistent rather than a physical parameter.

In the next step we will consider the effect of strain gradients on the SB initiation and propagation for homogeneous uniform deformation.

ORCID iDs

G Abeygunawardana-Arachchige  <https://orcid.org/0000-0001-8989-4132>

References

- Acharya A and Widom M 2017 A microscopic continuum model for defect dynamics in metallic glasses *Journal of the Mechanics and Physics of Solids* **104** 1–11 <https://www.sciencedirect.com/science/article/pii/S002250961630151X>
- Aifantis E C 1984 On the micro structural origin of certain inelastic models *J. Engng Mater. Tech.* **106** 326–34
- Argon A 1979 Plastic deformation in metallic glasses *Acta Metall.* **27** 47–58
- Bazant Z P 1976 Instability, ductility, and size effect in strain softening concrete *J. Eng. Mech. Div.* **102** 331–44
- Bazant Z P and Jirásek M 2002 Nonlocal integral formulations of plasticity and damage: survey of progress *Journal of Engineering Mechanics* **128** 1119–49
- Cheng J and Ghosh S 2013 Computational modeling of plastic deformation and shear banding in bulk metallic glasses *Comput. Mater. Sci.* **69** 494–504
- Dai L, Yan M, Liu L and Bai Y 2005 Adiabatic shear banding instability in bulk metallic glasses *Appl. Phys. Lett.* **87** 141916
- Dai L H and Bai Y L 2008 Basic mechanical behaviors and mechanics of shear banding in BMGs *Int. J. Impact Eng.* **35** 704–16

- Dai L H 2012 Shear banding in bulk metallic glasses *Adiabatic Shear Localization: Frontiers and Advances* ed Dodd Bradley and Yilong Bai 2 (United States of America: Elsevier) 8 311–47 <https://www.elsevier.com/books/adiabatic-shear-localization/dodd/978-0-08-097781-29780080977812>
- Donovan P E 1988 A yield criterion for Pd₄₀Ni₄₀P₂₀ metallic glass *Acta Metall.* **37** 445–56
- Fleck N and Hutchinson J 1993 A phenomenological theory for strain gradient effects in plasticity *J. Mech. Phys. Solids* **41** 1825–57
- Fleck N, Muller G, Ashby M and Hutchinson J 1994 Strain gradient plasticity: theory and experiment *Acta Metall. Mater.* **42** 475–87
- Greer A L, Cheng Y Q and Ma E 2013 Shear bands in metallic glasses *Materials Science and Engineering: R: Reports* **74** 71–132
- Jiang M and Dai L 2009 On the origin of shear banding instability in metallic glasses *J. Mech. Phys. Solids* **57** 1267–92
- Li Q and Li M 2007 Free volume evolution in metallic glasses subjected to mechanical deformation *Materials Transactions* **48** 1816–21
- Liu Y H, Liu C T, Gali A, Inoue A and Chen M W 2010 Evolution of shear bands and its correlation with mechanical response of a ductile Zr₅₅Pd₁₀Cu₂₀Ni₅Al₁₀ bulk metallic glass *Intermetallics* **18** 1455–64
- Lu X, Wang M, Du Y and Liao W 2018 Anisotropy in a bulk metallic glass induced by uni-directional heat flow *J. Non-Cryst. Solids* **486** 47–51
- Maaß R and Derlet P M 2018 Micro-plasticity and recent insights from intermittent and small-scale plasticity *Acta Mater.* **143** 338–63
- Narayan R L, Raut D and Ramamurty U 2018 A quantitative connection between shear band mediated plasticity and fracture initiation toughness of metallic glasses *Acta Mater.* **150** 69–77
- Nekousov V, Doak S, Roy A, Kuhn U and Silberschmidt V V 2018 Experimental studies of shear bands in Zr Cu metallic glass *J. Non-Cryst. Solids* **484** 40–8
- Nelson D R 1983 Order, frustration, and defects in liquids and glasses *Phys. Rev. B* **28** 5515
- Qu X, Huang M, Gu X and Lu X 2015 Numerical Implementation of non-local Mohr-Coulomb model. *Computer Methods and Recent Advances in Geomechanics* ed Oka Fusao, Akira Murakami, Ryosuke Uzuoka and Sayuri Kimoto 1 (London, UK: CRC Press) 187–92 9781138001480
- Rolshoven Simon and Jirasek Milan 2003 *Nonlocal plasticity models for localised failure* Swiss Federal Institute of Technology <https://infoscience.epfl.ch/record/33362/>
- Spaepen F 1977 A microscopic mechanism for steady state inhomogeneous flow in metallic glasses *Acta Metall.* **25** 407–15
- Strömberg L and Ristinmaa M 1996 FE-formulation of a nonlocal plasticity theory *Comput. Methods Appl. Mech. Eng.* **136** 127–44
- Toi Y, Lee J and Taya M 2004 Finite element analysis of superelastic, large deformation behavior of shape memory alloy helical springs *Computers & Structures* **82** 1685–93
- Tvergaard V and Needleman A 1995 Effects of non-local damage in porous plastic solids *Int. J. Solids Struct.* **32** 1063–77
- Vaidyanathan R, Dao M, Ravichandran G and Suresh S 2001 Study of mechanical deformation in bulk metallic glass through instrumented indentation *Acta Mater.* **49** 3781–9
- Xie X, Lo Y-C, Tong Y, Qiao J, Wang G, Ogata S, Qi H, Dahmen K, Gao Y and Liaw P 2018 Origin of serrated flow in bulk metallic glasses *J. Mech. Phys. Solids* **124** 634–42
- Yang Q, Mota A and Ortiz M 2006 A finite-deformation constitutive model of bulk metallic glass plasticity *Computational Mechanics* **37** 194–204
- Yu C-C, Chu J P, Jia H, Shen Y-L, Gao Y, Liaw P K and Yokohoma Y 2017 Influence of thin-film metallic glass coating on fatigue behaviour of bulk metallic glass: experiments and finite element modeling *Materials Science and Engineering: A* **692** 146–55
- Zhang Z F, Eckert J and Schultz L 2003 Difference in compressive and tensile fracture mechanisms of Zr₅₉Cu₂₀Al₁₀Ni₈Ti₃ bulk metallic glass *Acta Mater.* **51** 1167–79